



## Ecomorphodynamics of oyster reefs and their influence on oyster reef morphology

Francesca Roncolato<sup>a,b</sup>, Thomas E. Fellowes<sup>a,b</sup>, Stephanie Duce<sup>c</sup>, Carolina Mora<sup>a,b</sup>, Oskar Johansson<sup>a,b</sup>, Indiana Strachan<sup>a,b</sup>, Ana B. Bugnot<sup>b,e,f</sup>, Katherine Erickson<sup>b,d</sup>, Will Figueira<sup>b,e</sup>, Paul E. Gribben<sup>b,d</sup>, Christopher Pine<sup>b,e</sup>, Bree Morgan<sup>a,b</sup>, Ana Vila-Concejo<sup>a,b,\*</sup>

<sup>a</sup> Geocoastal Research Group, School of Geosciences and Marine Studies Institute, University of Sydney, Australia

<sup>b</sup> Sydney Institute of Marine Science, Chowder Bay, Sydney, Australia

<sup>c</sup> College of Science and Engineering, James Cook University, Bebegu Yumba Campus, Townsville, Queensland, Australia

<sup>d</sup> Centre for Marine Science and Innovation, University of New South Wales, Sydney, NSW, Australia

<sup>e</sup> School of Life and Environmental Sciences, University of Sydney, Sydney, NSW, Australia

<sup>f</sup> CSIRO Environment, St Lucia 4067, QLD, Australia

### ARTICLE INFO

#### Keywords:

Wave dissipation  
Wave exposure  
Oyster reef morphology  
Estuary  
Gamay  
Botany Bay  
Port Hacking  
Crookhaven

### ABSTRACT

Over 85 % of oyster reefs have been lost globally due to disease, overharvesting, global warming, and pollution. Consideration of the ecosystem services provided by healthy oyster reefs (e.g., coastal protection, water purification and carbon burial) has driven recent research and restoration efforts worldwide. However, hydrodynamic studies, specifically looking at the effects of different levels of wave exposure on the ecomorphodynamics of oyster reefs, are scarce. In this study, we consider oyster reefs in microtidal estuaries under different levels of relative wave exposure to determine how hydrodynamics may shape reef morphology and how reef morphology affects wave dissipation. We quantify oyster reef morphology through spatial analysis, using morphometrics and spatial density and relate these to the ability of oyster reefs to dissipate wave energy. Field campaigns were undertaken at three microtidal sites in southeast Australia with different hydrodynamic exposure and morphology: Gamay (Botany Bay), Port Hacking and Crookhaven River. We found that reef morphology and orientation is related to estuarine hydrodynamic conditions and thus we propose an ecomorphodynamic model with a continuum of morphologies from sparse reefs aligned perpendicular to the tidal currents and incoming waves (patch reefs), through broken up barriers semi-aligned or obliquely to the tidal flows (string reefs), to the total barrier that exists under the lowest hydrodynamic conditions (fringing reefs). The highest dissipative ability of locally generated wind waves occurred at Crookhaven (patch reef, 165 kW/m<sup>2</sup>), and lowest at Gamay (string reef, 11.66 kW/m<sup>2</sup>). Our results suggest that reef morphology, and orientation to currents and waves, influence wave dissipation, and that hydrodynamic conditions in turn influence reef morphology. These findings are important to inform future reef restoration under increasingly severe climate change conditions to optimise ecosystem services on restored oyster reefs.

### 1. Introduction

Oyster reefs are important habitat structures that are formed by dense aggregations of oysters settling on hard substrates. Oysters are important ecosystem engineers, providing services that hold socio-economic, recreational and ecological significance (Tolley and Volety, 2005; Beck et al., 2001; Grabowski et al., 2012; zu Ermgassen et al., 2013). Oysters are filter feeders, therefore improving water quality,

increasing light availability to benthic plants. In consequence, they increase energy transfer up the trophic levels promoting productivity within the ecosystem and an overall increase in estuarine health (Fodrie et al., 2017; Beck et al., 2001; Grabowski et al., 2012; zu Ermgassen et al., 2013). Oysters accrete upwards and sideways, making up reef structures that provide habitat for crustaceans, other molluscs and provide protection for fish species (Gutiérrez et al., 2003; Quan et al., 2009). As physical structures, these reefs dissipate wave energy and

\* Corresponding author at: Geocoastal Research Group, School of Geosciences and Marine Studies Institute, University of Sydney, Australia.  
E-mail address: [ana.vilaconcejo@sydney.edu.au](mailto:ana.vilaconcejo@sydney.edu.au) (A. Vila-Concejo).

<https://doi.org/10.1016/j.geomorph.2024.109213>

Received 19 October 2023; Received in revised form 17 April 2024; Accepted 18 April 2024

Available online 22 April 2024

0169-555X/© 2024 The Authors. Published by Elsevier B.V. This is an open access article under the CC BY license (<http://creativecommons.org/licenses/by/4.0/>).

mitigate shoreline erosion within estuaries, services which are conservatively valued at between \$5500 and \$99,000 per hectare (Grabowski et al., 2012).

However, oysters are sensitive to changing environmental conditions, particularly increases in temperature and acidification, tolerate water temperatures up to 30 °C and pH levels between 6.75 and 8.75. Changes to these preferred conditions can reduce oyster calcification rates and slow their growth (Marshall et al., 2021; Garner et al., 2022; Shumway et al., 1996). Water movements, currents and depth can also influence oyster survival, impacting their ability to filter feed influencing reef consolidation, dislodgement and morphology (Byers et al., 2015).

Oyster reefs dominated by Sydney Rock oysters are found in the temperate waters of Australia's eastern and southern coastline, specifically in shallow estuarine environments (Beseres Pollack et al., 2021). Estuaries are semi-enclosed bodies of water where the sea meets the land, and on the SE coast of Australia they can be categorised into three main types based on geological criteria: tide-dominated, wave-dominated and intermittently closed (Roy et al., 2001; Kennedy, 2016). Tide-dominated estuaries develop along protected shorelines due to sediment filling up a basin and prograding seawards, and commonly have low energy hydrodynamic conditions. These environments can occasionally be subject to fluvial and ocean surges, storm swell and infragravity waves (low frequency surface gravity waves) that increase the hydrodynamic conditions (Spicer et al., 2019). Wave-dominated estuaries evolve due to shore-parallel sand banks developing over the embayment entrance that continue to accrete to above sea level restricting marine exchange and creating a high energy, wave-dominated environment as the river establishes a direct channel with the ocean (Roy et al., 1980; Ryan et al., 2003). Intermittently closed estuaries occur when the sill is high enough to block tidal exchange with the ocean (Roy et al., 2001), with the hydrodynamic conditions of these systems being highly variable depending on whether the system is open or closed (Harvey et al., 2013). While Sydney rock oysters occur in both tide-dominated and wave-dominated environments, how their survival and growth is impacted by these conditions remains unresolved.

Oyster reefs were once abundant, however their habitats have declined by 85 % globally due to overharvesting, pollution, climate change and disease, (Kitsikoudis et al., 2020; Beck et al., 2011; Cook et al., 2022). Climate change alters site suitability for oysters due to rising sea levels, increasing water temperatures, acidification, and increasing severity and number of storms (Fodrie et al., 2014; Beck et al., 2011; Halpern et al., 2008; Lemasson et al., 2017). These changing coastline conditions increase the challenge of restoring oyster reefs and further accentuate the need to understand the relationship of reef design and hydrodynamics and wave exposure within the estuarine environment.

The relationship between oyster reef morphology and hydrodynamics in estuarine environments has been explored in recent studies. Wiberg et al. (2019), showed that the ability of oyster reefs to dissipate wave energy is dependent on mean sea level depth, and in deep water they are unable to provide coastline protection. Colden et al. (2016) used Grave's (1905, in Colden et al., 2016) oyster reef categories including patch reefs, string reefs, and fringing reefs and found that fringing reefs produced conditions that were conducive to reef persistence. Salvador de Paiva et al. (2018) analysed reef morphometrics and concluded that long and narrow reefs were the most successful in mitigating long-term coastal erosion. Wave exposure, specifically dominant wave direction, has also been examined in relation to oyster reefs' sediment accretion and stabilisation which impacts oyster distribution (Meyer et al., 1997; Theuerkauf et al., 2017). However, there is a gap in understanding the impacts of estuarine physiographic factors on morphodynamics of oyster reefs, specifically, for estuaries with varying wave exposure levels from wave protected, semi-protected and exposed. Resolving this gap could help inform reef design for oyster restoration projects in different hydrodynamic conditions with varying wave

exposure levels.

In this study we aim to understand ecomorphodynamics of oyster reefs by studying the role that oyster reef structures play in wave dissipation and how this is influenced by the reef's morphology. To achieve this, we investigated (1) the effect of different levels of wave exposure (exposed, semi-protected and protected) in estuarine environments, (2) the interrelationship between hydrodynamics and oyster reef morphology, and, (3) how dissipation of wave energy by oyster reefs was impacted by the factors listed above.

## 2. Backgrounds and methods

### 2.1. Study areas

This study focuses on field data collected at oyster reefs situated in three estuaries along the SE coast of Australia (Fig. 1): Gamay (Aboriginal name for Botany Bay, 151°10'50.77" E, 34°00'57.16" S) in 2018, Port Hacking (151°07'14.76" E, 34°04'24.55" S) in 2019, and Crookhaven River estuary (150°44'42.33"E, 34°54'22.83"S) in 2022. The New South Wales (NSW) coastline is highly embayed (184 estuaries) with a moderately deep and narrow continental shelf which greatly influences estuarine entrances and the ability for waves to propagate into the bays (Short and Trenaman, 1992; Hughes et al., 2019). The coast is swell dominated with mean significant waves height ( $H_s$ ) of 1.6 m and a period of 8 s from a SE direction; the coast regularly experiences storm waves defined by  $H_s > 3$  m (Short and Trenaman, 1992). At Crookhaven, mean significant wave heights exceeds 1.5 m 50 % of the time, and is  $>5$  m, 3 % of the time as described by Wright (1976). Typical wave climate conditions on the NSW coastline are influenced by seasonal changes with mid-latitude cyclones and low-pressure systems more common in Winter and in Summer calmer wave climates with lower significant wave height and shorter wave period (Harley et al., 2010; Gallop et al., 2020). All three estuaries are microtidal and exposed to different levels of relative wave exposure and pressure from urbanisation, resulting in pollution from stormwater runoff and development (Reid, 2020).

#### 2.1.1. Gamay

Gamay is a semi-enclosed, ocean embayment estuary (Roy, 1994), located 16 km south from Sydney (Fig. 1B) and includes the Towra Point Nature Reserve where the oyster reefs in this study are located. It is a tide-dominated system, experiencing micro tidal and semi-diurnal tides (range 1 m neap tides –1.9 m spring tides) and tidal current from N, at a maximum speed of 0.64 m/s (Bryant, 1980). The estuary opening is SE facing and protected by headlands allowing low energy hydrodynamic conditions on the oyster reefs, categorised as a semi-protected level of wave exposure. Wind speeds from Sydney Airport Weather Station (~2 km from Gamay) range from an annual mean 9 am wind speed of 14.2 km/h to annual mean 3 pm wind speed of 21.6 km/h (BOM, 2023). Historically winds in May are predominantly NW and W at 9 am and S at 3 pm, with  $>40$  km/h winds typically from the S, and occasionally E (BOM, 2023).

The Gamay oyster remnant reef, consisting of mostly *S. glomerata*, expands across the entrance of a small sub-embayment (Fig. 1E) and is comprised of over 150 structures. In this study 20 reef structures (out of 150) were surveyed as these structures represent the centre cluster of the reef. The others sparsely positioned outlying reefs (data collected using Google Earth Pro 7.3; Table 1). The natural reef has degraded significantly due to overfishing and dredging in the late 1800s - early 1900s (Gillies et al., 2020). The sediments are still quite polluted due to its proximity to Sydney Airport, Port Botany ~2.5 km away and high urban stormwater runoff from Cooks and Georges Rivers (Spooner et al., 2003; Jahan and Strezov, 2019). Recently, efforts have been made at this site to restore the remnant oyster reef habitat and reinstate ecosystem services and critical habitat.

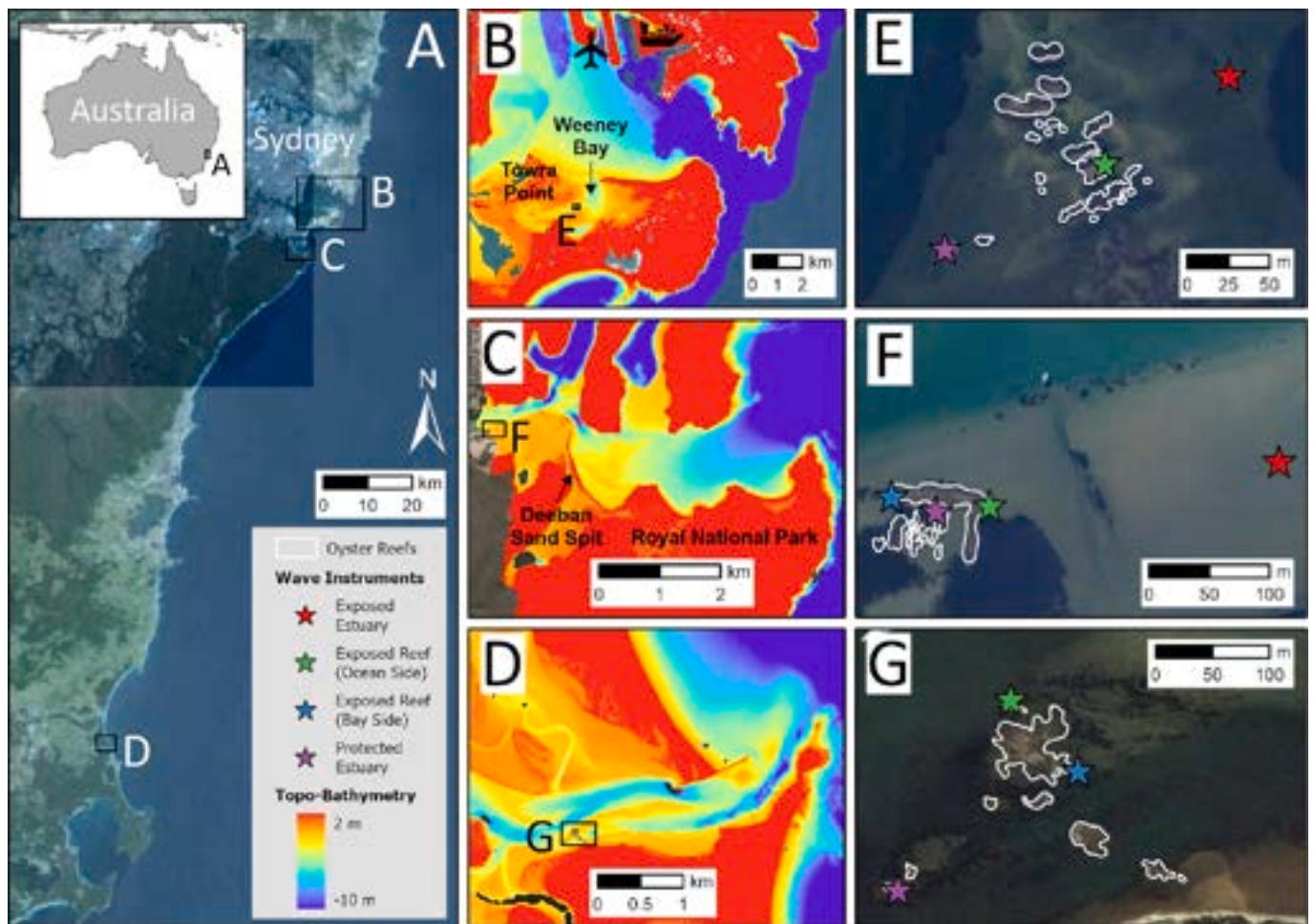


**Fig. 1.** Study areas in (A) SE Australia showing (B) Gamay (Botany Bay), (C) Port Hacking and (D) Crookhaven, along with their topo-bathymetry. The oyster reefs within each site (outlined in grey) are shown in (E, F and G) with hydrodynamic instrument placements indicated using coloured stars, with red = exposed estuary, green = exposed reef (ocean side), blue = exposed reef (bay side) and purple = protected estuary. In (B), An airplane symbol signifies the Sydney Airport, while the boat symbol signifies Port Botany. Imagery sourced from DPE (2014) and digital elevation model from DPE (2019). (For interpretation of the references to colour in this figure legend, the reader is referred to the web version of this article.)

**Table 1**

Morphometrics of oyster reefs. Average rugosity (derived from 3D modelling) area and perimeter (derived from Google Earth Pro) the other morphometric values were obtained using ArcGIS Pro (version 10.9.1).

Site	Reef Type	No. of Reefs	Av. Distance reef to reef (m)	Av. Surface area of individual reefs (m <sup>2</sup> )	Total Surface Area (m <sup>2</sup> )	Total Perimeter (m)	Average Rugosity	%Reef coverage in polygon	Orientation (degrees from North)
Gamay	String Reef	20	4.70	53.58	1178.90	630.36	1.53	19.54	26.61
Port Hacking	Fringe Reef	13	1.73	126.35	1642.56	599.91	1.82	47.28	72.15
Crookhaven	Patch Reef	10	10.03	237.23	2609.49	661.97	1.45	15.23	87.21

### 2.1.2. Port Hacking

Port Hacking is a tide-dominated, drowned valley estuarine system (Roy, 1994) located 30 km south of Sydney (Fig. 1A) with a low fluvial input depositing 1–2 mm/y (Kench, 1999). The estuary entrance faces NE and may allow high hydrodynamic energy inside the outer estuary. The inner estuary, where the oyster reefs are located, is microtidal (range 0.2–1.9 m), and tide current from the NE with a speed of to 0.65 m/s (Taylor et al., 2013). The oyster reef is protected by a sand spit, part of the flood tide delta, as well as the outer headlands at estuary entrance (Fig. 1C). The wind conditions of Port Hacking are the same as Gamay, as the closest weather station for both is Sydney Airport (BOM, 2023).

Historically winds in April are predominantly NW, W and S at 9 am and NE, SE and S at 3 pm, with >40 km/h winds predominantly from the S.

The oyster reef site is located 4 km upstream from estuary entrance, categorised as protected level of wave exposure (Fig. 1C). It is a small structure comprising approximately 13 separate structures (Fig. 1F; Table 1). This system is a naturalised remnant reef consisting of mostly *S. glomerata* (>90%; Leong et al., 2022) that has grown on top of ballast stones that were placed when the site was used as a port during the 1850s (Albani and Cotis, 2013). At present, the reef is somewhat protected from dense urbanisation and subsequent pollution, as it is located within a National Park reserve (Birch et al., 2021).

### 2.1.3. Crookhaven

The Crookhaven estuary is a wave-dominated, barrier river estuary (Roy, 1994), located 100 km south of Sydney (Fig. 1A). Tides are semidiurnal with significant diurnal inequality, with mean ranges of 1.2–1.8 m. The Crookhaven entrance is situated on a high energy coastline, facing NE, with a high level of wave exposure (Fig. 1D). Crookhaven's positioning on the coastline allows for the penetration of occasional large coastal storms inclusive of East Coast Lows causing flooding and inundation (Wright, 1976; Kumbier et al., 2018). However, typical conditions at this site, include wind speeds (measured at Nowra Weather Station ~21 km from Crookhaven) range from an annual mean 9 am wind speed of 14.3 km/h to annual mean 3 pm wind speeds of 20 km/h (Nowra Station, BOM, 2023). On average wind direction in March is dominated by NW and S winds at 9 am and E winds at 3 pm.

The oyster reef is located 1.5 km from the entrance and consists of nine structures on the south side of the estuary (data collected using Google Earth Pro 7.3, Fig. 1G; Table 1). These remnant reefs are comprised of mostly *S. glomerata* (>90 %) growing upon rocky and sandy substrate (Leong et al., 2022). This area experiences a moderate level of anthropogenic disturbances due to recreational use of the estuary, and storm water run-off according to the 2015–16 assessment of estuary health by the (NSW Department of Planning and Environment, 2016).

## 2.2. Field campaigns

Data were collected during three field campaigns at Gamay (30/04/2018–23/05/2018), Port Hacking (27/03/2019–26/04/2019) and Crookhaven (16/03/2022–28/03/2022). Three to four pressure transducers (RBR solo3) were deployed at each location around the reef at the estuary entrance, exposed, and protected positions measuring water pressure at frequencies between 2 and 8 Hz (Fig. 1E, F, G). A Real-time Kinematic – Global Navigation Satellite System (RTK-GNSS) measured elevation and locations of the RBR instrument deployments. RTK-GNSS and drone measurements were used for the Geospatial Analysis described in Section 2.3.

## 2.3. Geospatial analysis

### 2.3.1. Site characterisation

Each site was categorised into a reef type as described in the literature: (1) string reefs, characteristically similar to shoal reefs and orientated perpendicular to currents (2) fringe reefs, morphologically narrow, with lower elevation and often oriented perpendicular to tidal currents or situated along a channel and (3) patch reefs, morphologically consisting of small an irregular shaped individual structures, located near the mouth of a river (Colden et al., 2016; Boivin et al., 2018). Reef morphometrics were obtained using the *Measure* and *Polygon* tools in Google Earth Pro (Google Earth Pro 7.3, 2022) and 3-dimensional models developed with a structure-from-motion photogrammetry workflow using *Agisoft Metashape Professional* (v1.7; Agisoft LLC, 2021) as outlined in Figueira et al. (2015) and Leong et al. (2022). These measurements include surface area (m<sup>2</sup>), perimeter (m) and rugosity. Rugosity is a measurement of how complex a surface is (surface complexity), where greater values indicate more structurally complex surfaces and a value of one indicates a flat surface (Colden et al., 2017). This was calculated by dividing the 3D-reef area by the 2D-reef area on a given surface.

Spatial data calculated in ArcGIS Pro (version 10.9.1) included percentage reef surface area coverage (m<sup>2</sup>) within a convex polygon constructed using the *Minimum Bounding Tool* with a *Convex Hull Boundary*, reef orientation (using the orientation of the imagined line connecting the pair of vertices with the longest distance between them in the convex polygon) and mean closest distance from reef to reef (m). This data was compared to digital elevation models (DEMs) to understand the influence of the reef's morphometrics on the hydrodynamics of

the site.

### 2.3.2. Digital elevation models (DEMs)

DEMs were created for each of the three sites using RTK-GNSS elevation data, coupled with the NSW Marine LiDAR Topo-Bathy 2018 layer available from the ELVIS portal (© State Government of NSW and Department of Planning and Environment 2019) and drone data where available. At Port Hacking and Crookhaven structure from motion algorithms were used to reconstruct a digital surface model from drone imagery which was geo-referenced using RTK-GNSS data. No drone survey was conducted at Gamay due to flying restrictions because of airport proximity. Refer to Supplementary materials for more detail on the creation of the DEMs at each site.

## 2.4. Hydrodynamic analysis

Waves were analysed using standard spectral techniques with Fast Fourier Transformation (FFT) (Holthuijsen, 2007). The parameters calculated included mean depth of the instrument, significant wave height (H<sub>s</sub>) and peak wave period (T<sub>p1</sub>) for locally-generated wind waves defined as 1 to 4 s (1–0.25 Hz), swell waves 4 to 20 s (0.25–0.05 Hz), and infragravity waves 20–300 s (0.05–0.003 Hz) (Rahbani et al., 2022). Wave period results are included in the supplementary information (Figs. S1–S3).

We calculated dissipation rates across the reefs using shallow water wave energy and power and equations (Masselink et al., 2011). Wave energy was calculated using:

$$E = \frac{1}{8} \rho g H_s^2 \quad (1)$$

where,  $E$  is mean wave energy density per unit horizontal energy (J/m<sup>2</sup>);  $\rho$  is density of seawater (1027 kg/m<sup>3</sup>);  $g$  is gravity constant (9.8 m/s<sup>2</sup>);  $H_s$  is significant wave height. Wave power was calculated at three locations in each site, using Energy calculated from Eq. (1) and speed:

$$P = E C_g \quad (2)$$

where,  $P$  is wave energy flux (power) per unit length (kW/m<sup>2</sup>);  $E$  is energy (as above);  $C_g$  is speed of the wave group, calculated as  $\sqrt{gh}$  following the shallow water approximation of linear wave theory. Wave dissipation was calculated using eq. (2):

$$\text{Dissipation rate} = P_O - P_I \quad (3)$$

where,  $P_O$  is Power (exposed site),  $P_I$  is power (protected site).

Spectral field data was compared to offshore wave data including, significant wave height (H<sub>s</sub>), wave maximum height (H<sub>max</sub>), significant wave period (T<sub>z</sub>) and wave period correlated to highest energy peak (T<sub>p1</sub>) and wind direction data was acquired from Manly Hydraulics Laboratory Waverider bouys and Bureau of Meteorology.

## 3. Results

### 3.1. Geospatial analysis and characterisation of the oyster reefs at each site

#### 3.1.1. Gamay

The Gamay oyster reef is the smallest of the three sites included in this research. The surface area of the 20 structures included in our study totals ~1179 m<sup>2</sup> (Table 1). The studied standalone structures are relatively close together with an average separation of 4.7 m and a total percentage reef coverage within the study area of 19.5 % (Table 1). The average rugosity index of the reefs is 1.53, indicating that the reef surface has varying elevation (Table 1). The elevation of the tidal flat east, which is leeward, or downwind of the oyster reef, has a visibly larger area with a shallower elevation (> -0.59 to -0.53 m AHD) than the west side. This suggests sediment build up on the leeward side of the reef

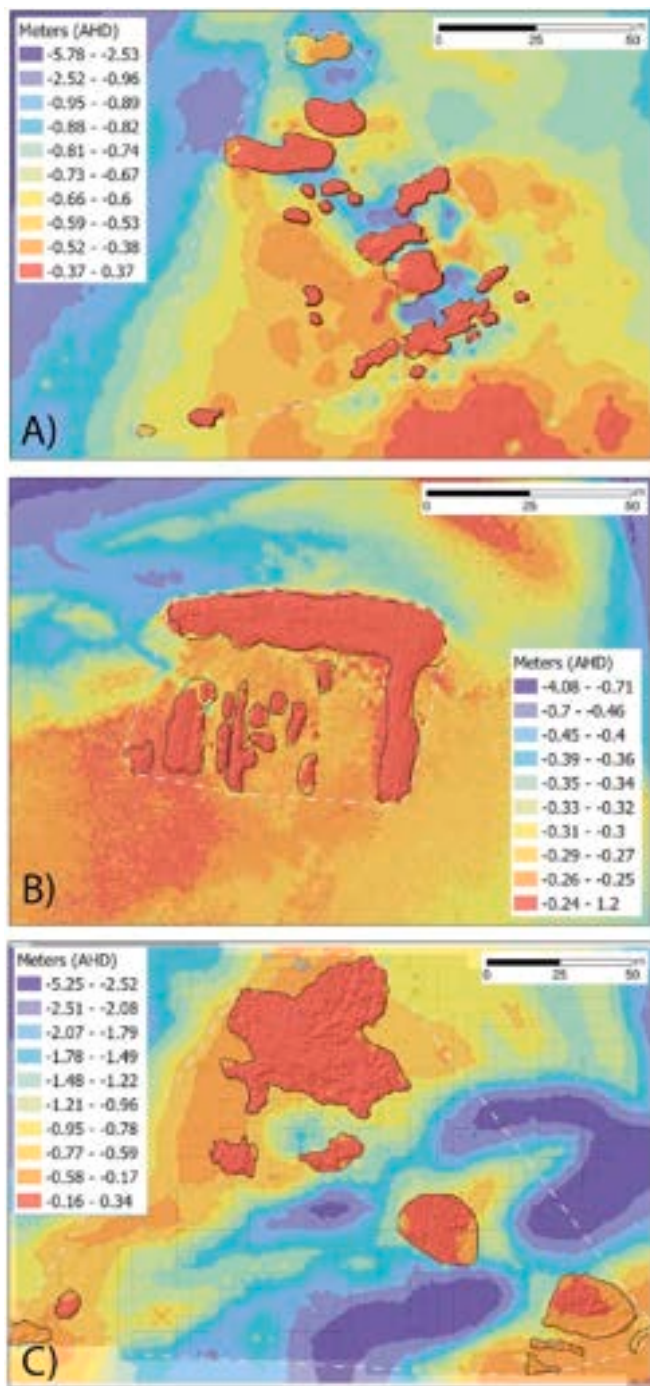


**Fig. 2.** Digital morphology models interpolated from elevation measurements at the A) Gamay, B) Port Hacking and C) Crookhaven study sites. Black outline indicates oyster reef structures and dashed grey outline indicates minimum convex polygon area. DEMs are displayed using 10 classes separated by quantiles such that each class has a different range and DEMs are not directly comparable.

(Fig. 2A). Maximum water depths occur in between reef structures and the East side of the reef ( $-5.78$  to  $-2.53$  m AHD) (Fig. 2A), possibly due to tidal currents. The reef has an orientation N-NE ( $26.6^\circ$ ), facing perpendicular to the channel (Table 1, Fig. 2a). The relatively deep inter-reef elevations and the small, standalone structures, classify the oyster reef at Gamay as a string reef (Fig. 2A).

### 3.1.2. Port Hacking

The oyster reef at Port Hacking, with a total surface area of  $1643 \text{ m}^2$ , comprises 13 standalone structures relatively close together with an average separation of  $1.7 \text{ m}$  and a total reef coverage within the study area of  $47.28 \%$  (Table 1). The average rugosity index of the reef patches is  $1.82$ , the highest index of the three sites, indicating the highest surface complexity with varying elevation across the reef (Table. 2). The DEM shows a relatively shallow area leeward of the reef ( $-0.26$  to  $-0.25$  m), suggesting sediment accumulates in this area, and sand shoals are increasingly shallow to the SW of the reef (Fig. 2B). Water depth increases immediately outside of the reef perimeter (N), where a channel runs alongside the structures (Fig. 2B). The reef is located on a shallow bank, parallel to the main estuary channel and acting as a barrier facing E-NE ( $72.15 \text{ deg}$ ) (Fig. 2B) and categorising this reef as a fringe reef (Table 1).

### 3.1.3. Crookhaven

Crookhaven reef covers an area of  $2609 \text{ m}^2$  (Table 1). It is comprised of the fewest standalone reef structures ( $n = 10$ ), with the largest average separation ( $\sim 10 \text{ m}$ ) and the lowest percentage of reef coverage within the study area ( $15 \%$ ) (Table 1). The average rugosity index of the reef patches is  $1.45$  which is the lowest index of the three sites, indicating that the surface of the reef is less complex (Table 1). The shallowest areas occur on the SW of the largest reef structure, ( $-0.58$  to  $-0.17$  m AHD, Fig. 2C) indicating an accumulation of sediment leeward from the reef in line with the entrance of the estuary (Fig. 1G). At the NE side of the reef the elevation is shallow ( $-0.58$  to  $-0.17$  m AHD, Fig. 2C) as the sediment is part of the flood tide delta extending towards the estuary entrance (Fig. 2C). The oyster reef is located near the mouth of the Crookhaven River, with an easterly orientation ( $87.21^\circ$ ) facing perpendicular to the main estuary channel (Fig. 1.G), categorising this as a patch reef.

## 3.2. Hydrodynamic analysis

### 3.2.1. Gamay

The Gamay reef is a protected site inside an estuary, and therefore the hydrodynamic conditions are influenced by locally generated winds, offshore swell and infragravity waves. During the study period there were N-NE winds on the 4th and 8th of May, as well as strong SW winds from the 12th to the 14th of May (Fig. 3A). Spectral energy density data indicates that the highest energy density occurred in the infragravity domain ( $>0.1 \text{ m}^2 \text{ Hz}^{-1}$ ), however energy density was also noticeable in the local wind wave domain (Fig. 6A). Overall  $H_s$  did not exceed  $0.1 \text{ m}$  at any of the Gamay sensors (Fig. 1).  $H_s$  for local wind waves fluctuated during the study period achieving four notable peaks ( $>0.05 \text{ m}$ ), the highest  $H_s$  was at the exposed estuary location ( $0.06 \text{ m}$ , Fig. 1E and 3C) due to local N-NE winds (Fig. 3A). Swell waves maintained small  $H_s$  ( $0\text{--}0.1 \text{ m}$ ) throughout the study period, with no significant peaks visible (Fig. 3D). On the 12th of May storm conditions were observed, causing SW winds and an increase in offshore maximum wave height from  $1.27 \text{ m}$  to  $6.9 \text{ m}$  in one day (Fig. 3B). The direction of these waves aligned with the ocean entrance to Gamay, allowing wave propagation into the estuary. Infragravity waves were recorded at all three pressure instrument locations around the reef, however, the highest significant wave height was observed at the exposed estuary,  $0.05\text{--}0.10 \text{ m}$  and, highlighted in blue Fig. 3E).

### 3.2.2. Port Hacking

Port Hacking is the most protected of the three study sites (Fig. 1). Winds during the study period originated mostly from the S-SE, apart from one occasion on the 31st of May when winds were coming from the NE (Fig. 4A). While there is a very low spectral energy density of  $>0.02 \text{ m}^2 \text{ Hz}^{-1}$  recorded at Port Hacking, while the highest density occurs between  $0$  and  $0.05 \text{ Hz}$  in the infragravity domain (Fig. 6B). However, most of the spectral energy density is distributed between  $0.45$  and  $1 \text{ Hz}$



**Fig. 3.** Wind speed and direction (a), offshore significant wave height ( $H_s$ ) and direction (b), wave height for local wind waves (c), swell waves (d) and infragravity waves (e) at Gamay (30/04/2018–24/05/2018). Locations: Exposed estuary/entrance (blue), exposed reef, ocean side (red) and protected (yellow). (For interpretation of the references to colour in this figure legend, the reader is referred to the web version of this article.)

in the local wind wave domain (Fig. 6B). Local wind wave  $H_s$  were small ( $<0.06$  m) across the entire site, with notable peaks predominantly evident at the exposed estuary, reaching  $H_s$  of 0.06 m on the 7th of April (Fig. 4C). At the exposed reef (ocean side) location there are two extraordinary peaks in  $H_s$  that occurred on the 14th of April and the 21st of April for both swell waves (0.034 and 0.030 m, respectively) and infragravity waves (0.15 and 0.13 m, respectively) (Fig. 4D and E).

### 3.2.3. Crookhaven

Crookhaven is the most exposed site in this study, with the oyster reef located close to the estuary entrance. During the field campaign at Crookhaven, NSW experienced the worst rain event in the last decade, resulting in significant rain events and flooding (BOM, 2023). Winds were predominately SW, reaching maxima of 30 km/h multiple times during the study period (Fig. 5A). The highest energy density occurred in the infragravity domain ( $>0.1$   $\text{m}^2 \text{Hz}^{-1}$ ); there are also smaller peaks in energy density in the wind wave and swell wave domains (Fig. 6C). Significant locally generated wind wave  $H_s$  increased over the 12 days, reaching a peak of 0.07 m on the 25th of March at the exposed reef (ocean side) location (Fig. 5C), coinciding with SW winds (Fig. 5A). Wind wave  $H_s$  peaked at the exposed reef (bay side) location a few days later, reaching 0.09 m on the 28th of March (Fig. 8C). Swell waves behaved similarly to wind waves, increasing in  $H_s$  over the 12-day period, with peaks of 0.09 m and 0.10 m at the exposed reef (bay side) location on the 25th and 28th of March respectively (Fig. 5D). Infragravity waves also peaked on the 28th of May at the exposed reef (bay side) location, recording  $H_s$  of 0.08 m (Fig. 5E). These spikes in hydrodynamic conditions coincided with increased rainfall and 30 km SSE winds from the 25th to 28th of March (Fig. 5A) (BOM, 2023). For all three wave types,  $H_s$  was larger at the two exposed locations, compared to the protected location (Fig. 5c, d and e).

## 3.3. Wave energy dissipation

### 3.3.1. Gamay

The wind wave dissipation rate between the exposed reef (ocean side) to the protected location shows three peaks, 11.66, 5.50 and 4.66  $\text{kW/m}^2$  (Fig. 7A). Coinciding with these peaks are three troughs (i.e., negative dissipation rates) between the exposed estuary and the exposed reef (ocean side) location. This indicates an increase in energy as the wind waves propagate from the estuary entrance to the exposed reef, of  $-12.51$ ,  $-8.83$  and  $-4.16$   $\text{kW/m}^2$  (Fig. 7A) followed by wave energy dissipation over the oyster reefs. Swell wave dissipation is unsurprisingly minimal across the site (Fig. 7B) given there is little to no energy density in the swell wave domain (Fig. 6A). In contrast, there is a less obvious pattern observed in the infragravity wave dissipation rate, however the magnitude of dissipation appears larger at the start and end of the instrument deployments (Fig. 7C), coinciding with the bigger infragravity waves recorded (Fig. 3E).

### 3.3.2. Port Hacking

Wind wave dissipation peaked on the 8th of April, as the wave power increased from the exposed location, propagating towards the exposed reef (ocean side) with a dissipation rate of  $-21.82$   $\text{kW/m}^2$  (Fig. 7D). The energy decreased at a dissipation rate of  $28.87$   $\text{kW/m}^2$  from the ocean side to the bay side of the exposed reef (Fig. 7D). On the 15th of and 20th of April (Fig. 3A) the swell and infragravity waves propagated over the reef, with the wave energy increasing for swell and infragravity waves from the exposed estuary to the exposed reef (ocean side) locations, then dissipation over the exposed reef (bay side) location (Fig. 7E, F). Dissipation rates for infragravity waves were much higher than swell waves, at  $73.66$   $\text{kW/m}^2$  compared to  $3.71$   $\text{kW/m}^2$  on April 15th and  $46.51$   $\text{kW/m}^2$  compared to  $2.43$   $\text{kW/m}^2$  on April 20th (Fig. 7F).



**Fig. 4.** Wind speed and direction (a), offshore significant wave height ( $H_s$ ) and direction (b), wave height for local wind waves (c), swell waves (d) and infragravity waves (e) at Port Hacking (27/03/2019–26/04/2019). Locations: Exposed estuary/entrance (blue), exposed reef (ocean side) (orange), protected (purple) and exposed (bay side) (yellow). (For interpretation of the references to colour in this figure legend, the reader is referred to the web version of this article.)

### 3.3.3. Crookhaven

Wind wave dissipation peaked at  $39.90 \text{ kW/m}^2$  from the exposed reef (bay side) to the protected location on the 28th of March (Fig. 7G). The highest swell wave dissipation rate peaks can be observed from the 25th–27th predominately from the exposed reef (bay side) location to the protected location,  $32.78$  and  $36.98 \text{ kW/m}^2$  chronologically and at a lesser rate from the exposed reef (ocean side) location to protected location,  $19.79$  and  $19.97$  (Fig. 7H). Infragravity waves had a much higher dissipation rate when propagating to the protected location from the bay side of the exposed reef, rather than from the ocean side, for example  $26.68$  compared to  $-8.97 \text{ kW/m}^2$  on the 21st of March (Fig. 7I).

## 4. Discussion

### 4.1. Oyster reefs exist under varying wave regimes

In this study we show that oyster reefs occur under different wave exposure, and consequently the dominant wave types are different at an exposed (Crookhaven), a semi-protected (Gamay) and a protected (Port Hacking) estuary (Fig. 6). At wave exposed oyster reefs (Crookhaven) the hydrodynamics profile is primarily characterised by relatively large swell and infragravity waves,  $>0.1 \text{ m}$  (Fig. 5) with only a small contribution from locally-generated wind waves (Fig. 6C). Conditions observed at Crookhaven are typical of the mean wave climate despite the flooding event, this region experiences a highly variable wind wave climate, determined by seasonal changes and semi-regular flooding

events (Wright, 1976; Kumbier et al., 2018). At semi-protected oyster reefs (Gamay) the energy density contributions from waves are within local wind wave and infragravity domains (Fig. 6A), with heights of  $0.06 \text{ m}$  and  $0.1 \text{ m}$  respectively (Fig. 4). Our results indicate that infragravity waves can penetrate inside the estuary at both the exposed (Crookhaven), and semi-protected (Gamay) sites and influence the hydrodynamic conditions on oyster reefs, supporting the findings of Rahbani et al. (2022).

Importantly, for Gamay, we attribute the relatively high infragravity wave energy to a south-westerly storm from the 12 to the 14th May propagating waves through the estuary (Fig. 4A). Past studies in Gamay show that the hydrodynamic conditions in this area are typically influenced by locally generated wind waves, as well as swell generated waves, particularly during storms (Gallop et al., 2020; Vila-Concejo et al., 2020; Rahbani et al., 2022). At the protected oyster reefs (Port Hacking) hydrodynamic energy is mainly dominated by local wind waves (Fig. 6), with some notable peaks in the swell wave domain ( $>0.034 \text{ m}$  Fig. 6B). Gamay (semi-protected) had wave heights that fell between the large (often  $>0.1 \text{ m}$ ) waves of Crookhaven (exposed), and the small ( $<0.03 \text{ m}$  and  $0.15 \text{ m}$ ) waves at Port Hacking (protected), suggesting wave height decreased for more protected estuaries. This agrees with previous research that established different wave signatures for different estuarine beaches as a consequence of their location within the estuary (Rahbani et al., 2022) (Fig. 6). Categorising wave climates and hydrodynamic conditions in each exposure level is important, as it affects an oyster reef's ability to dissipate wave energy, specifically

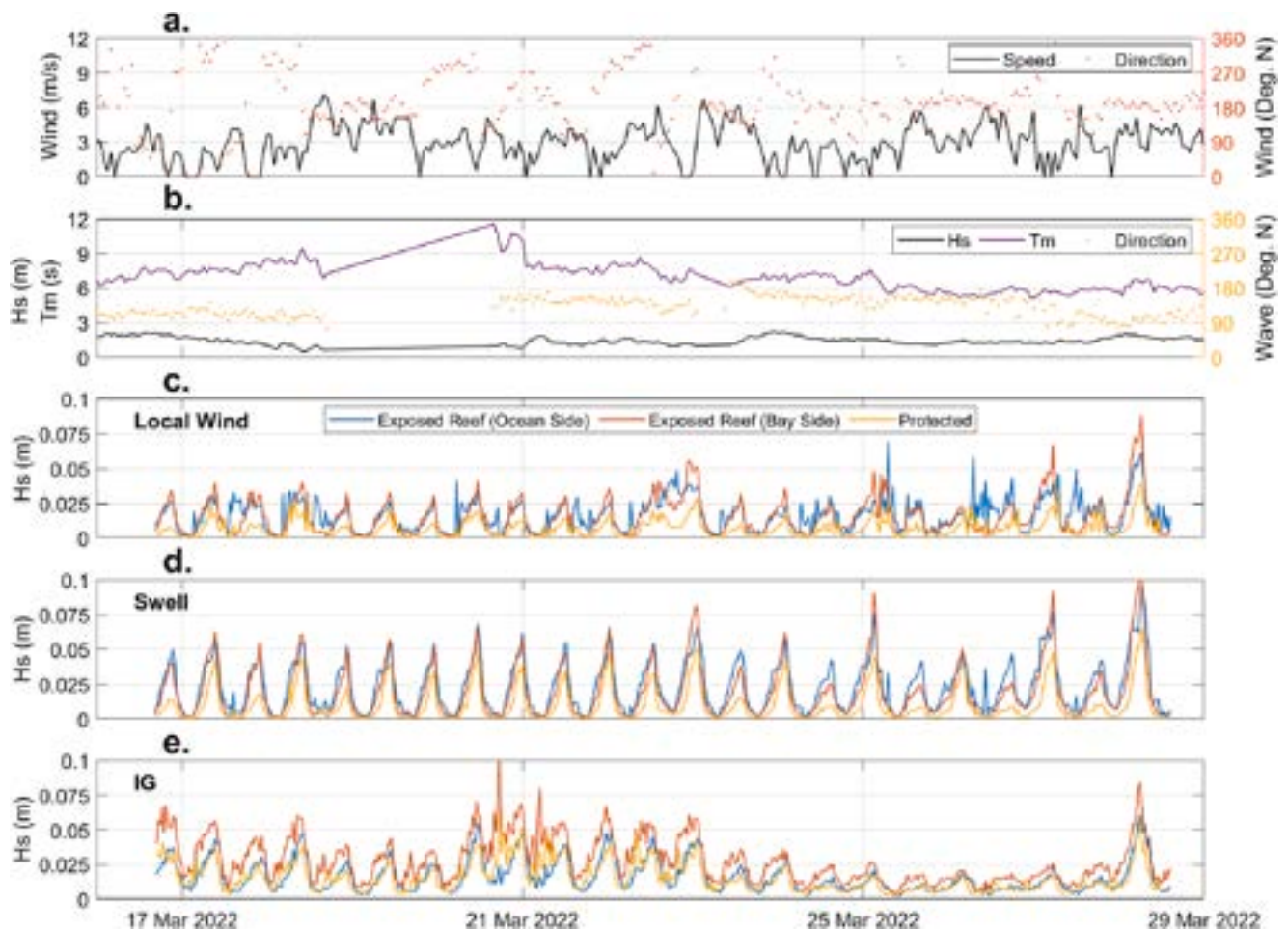


Fig. 5. Wind speed and direction (a), offshore significant wave height ( $H_s$ ), significant period ( $T_m$ ) and direction (b), wave height for local wind waves (c), swell waves (d) and infragravity waves (e) at Crookhaven from field campaign (16/03/2022–28/03/2022). Locations: Exposed (ocean side) (blue), exposed (bay side) (red) and protected (orange). (For interpretation of the references to colour in this figure legend, the reader is referred to the web version of this article.)

influenced by wave type and size (Zhu et al., 2020).

#### 4.2. Wave dissipation by oyster reefs

Previous work characterised oyster reefs based on their morphology (Grave, 1905 in Colden et al., 2016), as well as reef morphometrics, such as length and width (Salvador de Paiva et al., 2018). Rugosity has also been examined as a defining characteristic influencing wave dissipation (Kitsikoudis et al., 2020), however, contrastingly also as a factor that does not vary greatly between different oyster reefs. Accordingly, our results show the average rugosity is similar across the three sites, however as the index is  $>1$  at all three sites (Table 1) the influence of the reefs on hydrodynamics is likely to be greater than that of a perfectly smooth surface (Hearn, 2011). The oyster reefs in this study are morphologically categorised into Patch Reef, Fringe Reef, and String Reef (Crookhaven, Port Hacking and Gamay, respectively) (Table 1) partially following Grave (1905 in Colden et al. (2016)), however there are observed differences between the definitions provided in Colden et al. (2016) and the characterisation of each reef in this study (Boivin et al., 2018).

Crookhaven, a Patch Reef, is our most exposed site and aligned perpendicular to the current flow from the estuary mouth (shore-normal alignment), which increases the ability of a reef to dissipate energy. The reef is located close to the mouth of the estuary in deeper water (Fig. 2), as described in Colden et al. (2016), however the description of patch reefs usually forming in areas lacking strong bidirectional currents, is not the observation in this study. Coral patch reefs, as described in

Boivin et al. (2018), are found in sites characterised by high hydrodynamic conditions, which is similar to what was observed at Crookhaven. This study demonstrates that high dissipation rates for locally generated wind waves reached maxima of  $165 \text{ kW/m}^2$  from the exposed reef (bay side) to the protected location (Fig. 7G). Swell waves and infragravity waves presented lower dissipation rates over the reef ( $<39$  and  $26.77 \text{ kW/m}^2$ , respectively), which is notable as these waves had the highest heights (Fig. 5C and E). Gamay has a relatively low elevation with a high of  $0.34 \text{ m ADH}$  (Fig. 3A). Morris et al. (2021) found that reef elevation is an important factor for optimising wave attenuation on oyster reefs, specifically that low reef elevation coupled with high mean water levels result in inundation of reefs and minimal wave dissipation. While Morris et al. (2021) study was looking at reefs in deep water ( $\sim 5 \text{ m}$  water depths), the same principle underpins the dissipation rates at Gamay, with resulting low wind wave dissipation rates observed,  $>11.66 \text{ kW/m}^2$  from the exposed reef (ocean side) to the protected location (Fig. 7A).

The oyster reef at Port Hacking is a barrier reef and therefore expected to have a high dissipative ability according to Colden et al. (2016). However, due to the protected nature of the site, the oyster reef presents low dissipation rates, as the wave energy is low, additionally demonstrating the ability of fringing (barrier) reefs to form in lower hydrodynamic conditions (La Peyre et al., 2015; Borsje et al., 2011; Morris et al., 2021). This is evident in the dissipation rates calculated for locally generated wind waves, which are much lower at Port Hacking than at Crookhaven. The oyster reef at Port Hacking was able to dissipate the largest waves that propagated through the site, contradicting the findings from Wiberg et al. (2019), who showed that fringing reefs

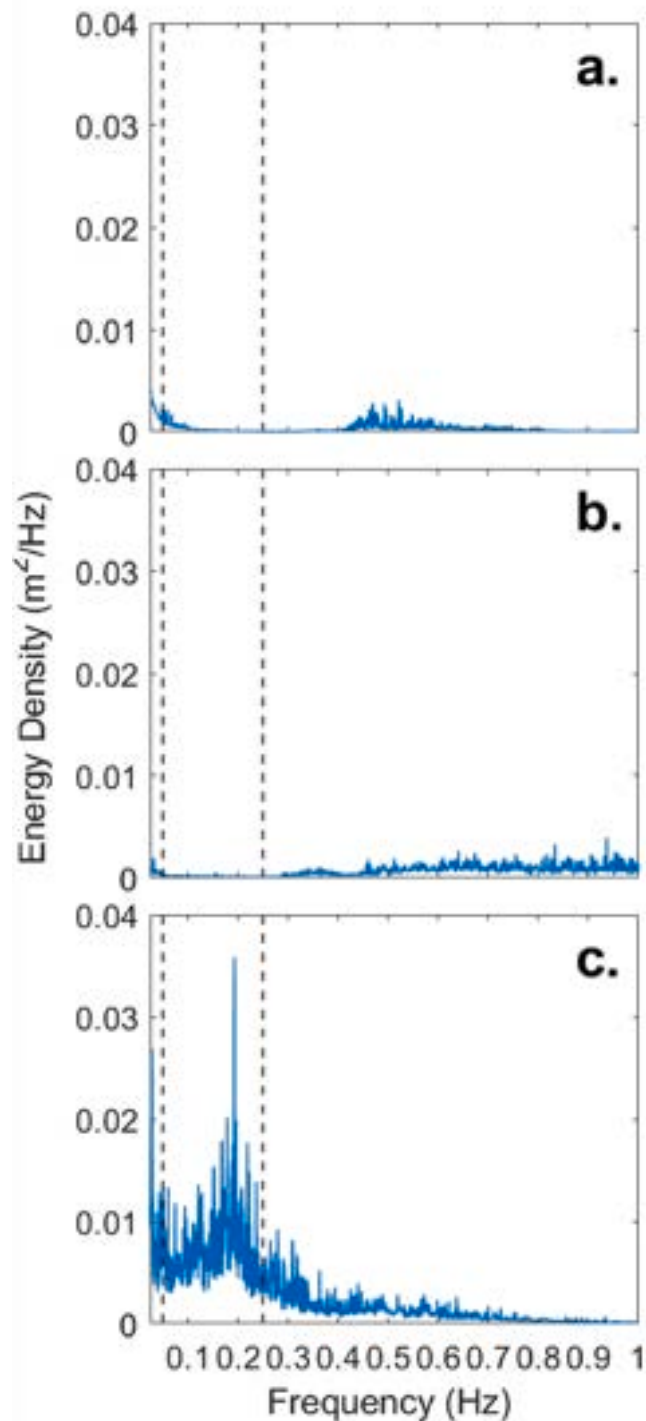


**Fig. 6.** Spectral energy density at Gamay (a), Port Hacking (b), Crookhaven (c). Different wave types are within each frequency range, wind waves (1–0.25 Hz), swell waves (0.25–0.05 Hz), and infragravity (0.05–0.003 Hz).

have little effect on wave attenuation of large waves. These results can be attributed to the maximum depth being greatest at Port Hacking, and lowest at Crookhaven, as well as the continuity of the reef at Port Hacking acting as a barrier. Our results show that oyster reef morphology, morphometrics and spatial placement within an estuary are important driving factors in changing hydrodynamic conditions and wave dissipation capabilities, influenced by different wave exposures

(Theuerkauf et al., 2017; Morris et al., 2021; Wall et al., 2005).

#### 4.3. An ecomorphodynamic conceptual model for oyster reefs

Patch reefs (e.g., Crookhaven), as defined in this study, can be characteristic of sites that are exposed to hydrodynamic energy, and thus experience strong tidal currents and high wave heights. The combination of waves and tidal flows play a key role in larvae distribution (Stagličić et al., 2020), which result in a reef that is predominately aligned to the incoming currents and waves, perhaps reflecting the direction of larval transportation before settling. The high energy experienced by patch reefs may reduce the ability for the larvae to settle and thus levels of larval recruitment may be low (Whitman and Matthew, 2012). On the other side of the spectrum, fringing reefs (e.g., Port Hacking) exist under low hydrodynamic settings. We hypothesise that the weak hydrodynamics allow larval settlement and the formation of a continuous barrier that further protects the low energy ecosystem behind it, allowing for sediment accumulation and facilitating the hydrodynamic regime suitable for extensive seagrass establishment and growth (Smith et al., 2009; Ridge et al., 2017). In this case, the barrier runs parallel to the incoming currents and deflects small waves propagating from the channel. Interestingly, the L-shaped branch of Port Hacking fringing reef might be related to the artificial structure underneath or to a secondary tide channel that runs perpendicular to the main channel near the reef. In any case, this branch of the reef is poorly developed when compared to the main barrier that runs along the main channel. String reefs (e.g., Gamay) are somewhere in between these two extremes of hydrodynamic conditions; they experience some tidal currents and small wave heights with some higher energy events in which storm waves propagate into the estuary, leading to a morphology consisting of many standalone structures, spatially widespread that is not completely aligned to incoming waves and currents, forming instead a broken barrier (Fig. 8). In this case, the milder hydrodynamic conditions may permit the larvae to settle perpendicular to the current flow (North et al., 2008).

Our ecomorphodynamic conceptual model (Fig. 8) proposes that oyster reef morphology and spatial density is influenced by the hydrodynamic conditions, particularly wave exposure and tidal currents. We hypothesise that there is a continuum of morphologies from sparse reefs perpendicular to the tidal currents and incoming waves (patch reefs), through broken up barriers semi-aligned to the tidal flows (string reefs), to the total barrier that exists under the lowest hydrodynamic conditions (fringing reefs). Furthering this, it can be inferred that reef morphology can influence the environment surrounding the reef, increasingly from patch to barrier. At Port Hacking (fringing reef) the sediment accumulation and thriving seagrass behind the barrier corroborates this hypothesis. Moreover, Bugnot et al. (2022) established that the bioturbation activity by large infaunal organisms in sediments surrounding oyster reefs, is influenced more greatly at a fringing reef (Port Hacking) than a string reef (Gamay).

#### 4.4. The importance of oyster reefs in present and future coastal protection

Our study demonstrates that oyster reefs are efficient in dissipating wave energy with high dissipation rates obtained for high wave exposure sites within estuaries. We show how reef morphology and spatial density is related to incoming waves and wave dissipation, and this is important because oyster reefs have been shown to reduce coastline hazards, such as shoreline erosion (La Peyre et al., 2015). The findings of this study are a step forward in understanding the ecosystem services of oyster reefs within estuaries in a range of wave exposed environments and how this is influenced by the morphology of the oyster reefs. Indeed, our results may be used to inform oyster reef design according to hydrodynamic conditions in future restorations. Further research is required to understand survivability of oyster reefs and potential erosion

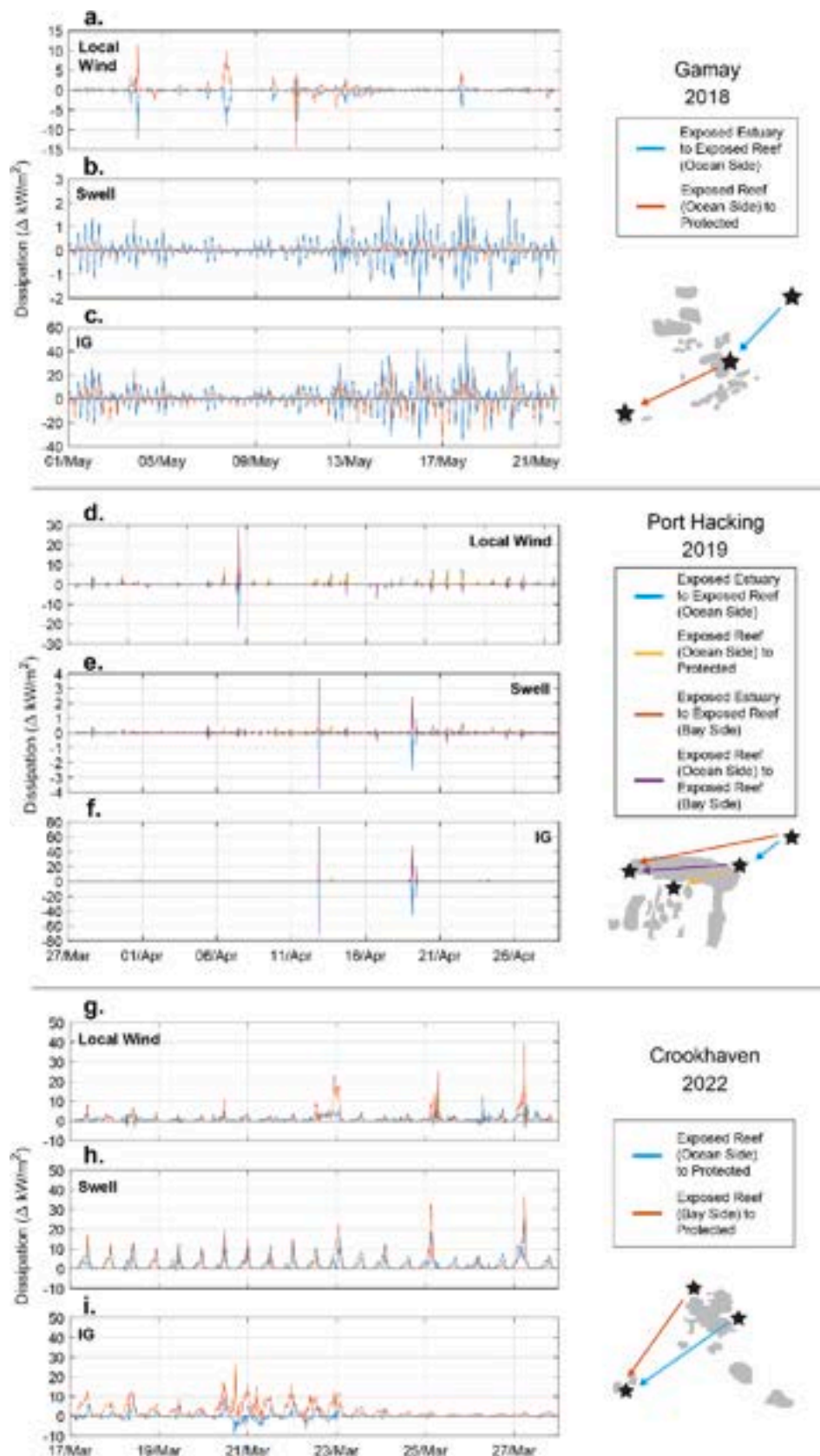


**Fig. 7.** Time series of dissipation rates between hydrodynamic instruments over oyster reefs at Gamay for local wind waves (a), swell waves (b) and infragravity waves (c), Port Hacking for local wind waves (d), swell waves (e) and infragravity waves (f) and Crookhaven for local wind waves (g), swell waves (h) and infragravity waves (i). Please note y-axis vary between wave types and locations with negative dissipation values denoting an increase in wave energy between the two instruments.

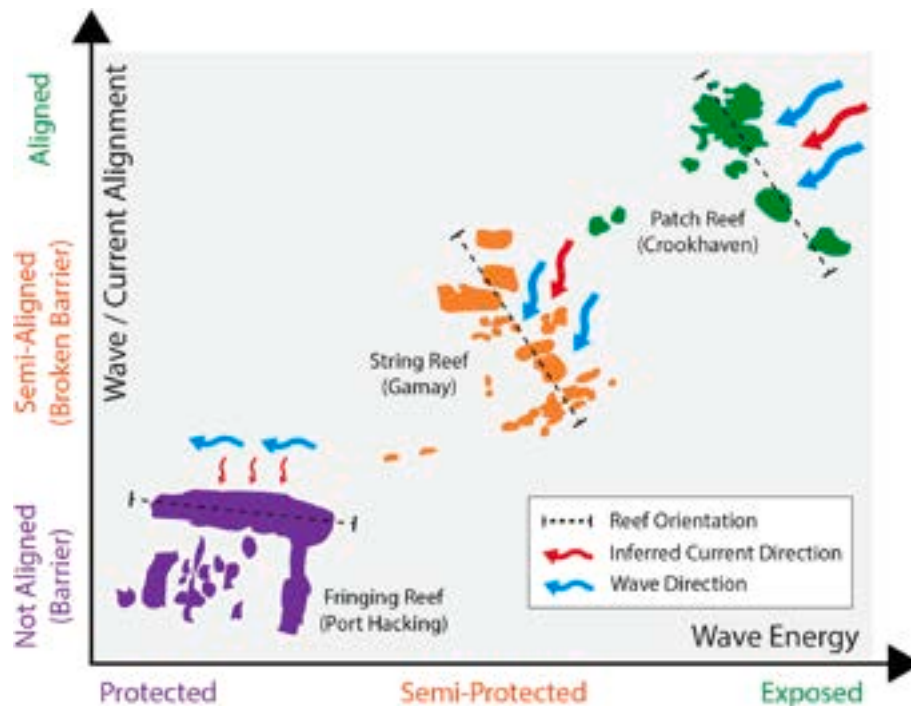


**Fig. 8.** Conceptual model highlighting varying reef morphology and current alignment, and the associated wave exposure and hydrodynamic conditions. Waves are aligned perpendicular to the reef for Crookhaven, obliquely aligned for Gamay and are parallel to Port Hacking (not aligned). The blue arrows represent the wave direction in the estuary and the red arrows represent the inferred current direction. (For interpretation of the references to colour in this figure legend, the reader is referred to the web version of this article.)

mitigation capabilities in changing environments. Majority of studies to date on oyster reef morphology focus on surface morphology, with little enquiry into the depth structure of these reefs (Walles et al., 2014; Salvador de Paiva et al., 2018). Future research should consider oyster reef structures depth and perhaps the substrate and formation of reefs. Future research should also include the impact of boat wakes as another driving factor in oyster reef ecomorphodynamics (Wall et al., 2005). Finally, we suggest that numerical modelling should complement future ecomorphodynamic studies to inform reef restoration and quantify wave dissipation capacity and other ecosystem services.

## 5. Conclusion

This study quantified the influence of wave exposure on oyster reefs in estuaries and their ability to dissipate wave energy. Hydrodynamic conditions and wave climates at oyster reefs are impacted by varying wave exposure at each site, with low swell-generated wave energy in protected sites (Port Hacking), and higher in more exposed sites (Crookhaven), infragravity waves propagating through Gamay during storm conditions, and wind waves present across all three sites. Arguably the most notable finding of this study is the interrelated nature of these varying morphologies with local hydrodynamics and wave dissipation within the estuary. The ecomorphodynamics of oyster reefs in these estuarine conditions can be represented in a continuum, from patch reefs, that are sparsely spread, and aligned with the currents at wave exposed sites (e.g., Crookhaven), to string reefs, aligned with the currents and creating broken barriers at the semi-protected site (e.g., Gamay), to fringing reefs, unaligned with the currents, creating a broken barrier at the protected site (e.g., Port Hacking). These morphologies have different dissipative abilities, for example, fringing, barrier reefs have the highest dissipative ability and facilitate the growth of different ecosystems on the protected side of the reef. Wave exposure also plays a role, with increased wave exposure causing higher wave dissipation rates, which was seen at the site with the highest level of exposure, Crookhaven, despite the morphological and spatial patch nature of the

reef. Based on the findings of this paper and climate change projections, future oyster reef restorations should consider ecomorphodynamics coupled with numerical modelling to understand suitable reef configurations and the associated wave dissipation capacity and other ecosystem services.

## CRediT authorship contribution statement

**Francesca Roncolato:** Writing – review & editing, Writing – original draft, Investigation, Formal analysis. **Thomas E. Fellowes:** Writing – review & editing, Writing – original draft, Supervision, Methodology, Investigation, Conceptualization. **Stephanie Duce:** Writing – review & editing, Writing – original draft, Visualization, Methodology, Investigation. **Carolina Mora:** Methodology, Investigation, Formal analysis. **Oskar Johansson:** Methodology, Formal analysis. **Indiana Stratchan:** Investigation, Formal analysis. **Ana Bugnot:** Writing – original draft, Project administration, Methodology, Funding acquisition, Conceptualization. **Katherine Erickson:** Writing – original draft, Resources, Project administration, Methodology, Data curation. **Will Figueira:** Writing – original draft, Resources, Project administration, Funding acquisition, Formal analysis. **Paul E. Gribben:** Writing – original draft, Project administration, Funding acquisition. **Christopher Pine:** Writing – original draft, Methodology, Investigation, Formal analysis, Data curation. **Bree Morgan:** Writing – original draft, Methodology, Investigation, Formal analysis, Conceptualization. **Ana Vila-Concejo:** Writing – review & editing, Writing – original draft, Supervision, Project administration, Methodology, Investigation, Funding acquisition, Conceptualization.

## Declaration of competing interest

The authors declare that they have no known competing financial interests or personal relationships that could have appeared to influence the work reported in this paper.

## Data availability

Data will be available on a link

## Acknowledgements

We acknowledge the traditional custodians of the Aboriginal lands on which this research was conducted. Thank you to Tom Savage and Bernadeth Antonio for their laboratory assistance. Thank you to all the volunteers who assisted during many field campaigns at the three estuaries, this would not have been possible without you. This research was supported by the Maple Brown Foundation, and the Australian Research Council through a Linkage Grant (LP180100732) in partnership with The Nature Conservancy and the Department of Primary Industries of NSW, Australia.

## Appendix A. Supplementary data

Supplementary data to this article can be found online at <https://doi.org/10.1016/j.geomorph.2024.109213>.

## References

- Albani, A.D., Cotis, G., 2013. Port Hacking: Past and Present of an Estuarine Environment. Sutherland Shire Council and University of New South Wales.
- Beck, M.W., Heck, K.L., Able, K.W., Childers, D.L., Eggleston, D.B., Gillanders, B.M., Halpern, B., Hays, C.G., Hoshino, K., Minello, T.J., Orth, R.J., Sheridan, P.F., Weinstein, M.P., 2001. The identification, conservation, and management of estuarine and marine nurseries for fish and invertebrates. *BioScience* 51 (8), 633–641. <https://doi.org/10.1641/0006-3568>.
- Beck, M.W., Brumbaugh, R.D., Airolidi, L., Carranza, A., Coen, L.D., Crawford, C., Defeo, O., Edgar, G.J., Hancock, B., Kay, M.C., Lenihan, H.S., Luckenbach, M.W., Toropova, C.L., Zhang, G., Guo, X., 2011. Oyster Reefs at risk and Recommendations for Conservation, Restoration, and Management. *BioScience* 61 (2), 107–116. <https://doi.org/10.1525/bio.2011.61.2.5>.
- Beseres Pollack, J., Palmer, T.A., Williams, A.E., 2021. Medium-term monitoring reveals effects of El Niño Southern Oscillation climate variability on local salinity and faunal dynamics on a restored oyster reef. *PLoS One* 16 (8), e0255931. <https://doi.org/10.1371/journal.pone.0255931>.
- Birch, G.F., Lee, J.-H., Gunns, T., 2021. Baseline assessment of anthropogenic change and ecological risk of an estuary bordered by an urbanized catchment and a pristine national park (Port Hacking estuary, Australia). *Mar. Pollut. Bull.* 162, 111822. <https://doi.org/10.1016/j.marpolbul.2020.111822>.
- Boivin, S., Gretz, M., Lathuilière, B., Olivier, N., Bartolini, A., Martini, R., 2018. Coral- and oyster-microbialite patch reefs in the aftermath of the Triassic–Jurassic biotic crisis (Sinemurian, Southeast France). *Swiss J Geosciences* 111, 537–548. <https://doi.org/10.1007/s00015-018-0310-y>.
- BOM, 2023. Climate Statistics for Nowra RAN Air Station (1955–2000). Bureau of Meteorology, Commonwealth of Australia. Accessed 5/87/2023. [http://www.bom.gov.au/climate/averages/tables/cw\\_068076\\_All.shtml](http://www.bom.gov.au/climate/averages/tables/cw_068076_All.shtml).
- Borsje, B.W., van Wesenbeeck, B.K., Dekker, F., Paalvast, P., Bouma, T.J., van Katwijk, M.M., de Vries, M.B., 2011. How ecological engineering can serve in coastal protection. *Ecol. Eng.* 37 (2), 113–122. <https://doi.org/10.1016/j.ecoleng.2010.11.027>.
- Bryant, E., 1980. Bathymetric changes in three estuaries of the Central New South Wales coast. *Mar. Freshw. Res.* 31 (5), 553. <https://doi.org/10.1071/MF9800553>.
- Bugnot, A.B., Dafforn, K.A., Coleman, R.A., Ramsdale, M., Gibbeson, J.T., Erickson, K., Vila-Concejo, A., Figueira, W.F., Gribben, P.E., 2022. Linking habitat interactions and biodiversity within seascapes. *Ecosphere* 13 (4). <https://doi.org/10.1002/ecs2.4021>.
- Byers, J.E., Grabowski, J.H., Piehler, M.F., Hughes, A.R., Weiskel, H.W., Malek, J.C., Kimbro, D.L., 2015. Geographic variation in intertidal oyster reef properties and the influence of tidal prism. *Limnol. Oceanogr.* 60 (3), 1051–1063. <https://doi.org/10.1002/lno.10073>.
- Colden, A., Latour, R., Lipcius, R., 2017. Reef height drives threshold dynamics of restored oyster reefs. *Mar. Ecol. Prog. Ser.* 582, 1–13. <https://doi.org/10.3354/meps12362>.
- Colden, A.M., Fall, K.A., Cartwright, G.M., Friedrichs, C.T., 2016. Sediment Suspension and Deposition across Restored Oyster Reefs of varying Orientation to Flow: Implications for Restoration. *Estuaries and Coasts* 39 (5), 1435–1448. <https://doi.org/10.1007/s12237-016-0096-y>.
- Cook, P.A., Warnock, B., Gillies, C.L., Hams, A.B., 2022. Historical abundance and distribution of the native flat oyster (*Ostrea angasi*) in estuaries of the Great Southern region of Western Australia help to prioritise potential sites for contemporary oyster reef restoration. *Mar. Freshw. Res.* 73 (1), 48. <https://doi.org/10.1071/MF21058>.
- DPE, 2014. NSW Imagery. Department of Planning and Environment, State Government of New South Wales, Sydney.
- DPE, 2019. NSW Marine LiDAR Topo-Bathy 2018. Department of Planning and Environment, State Government of New South Wales, Sydney.
- Figueira, W., Ferrari, R., Weatherby, E., Porter, A., Hawes, S., Byrne, M., 2015. Accuracy and precision of habitat structural complexity metrics derived from under-ater photogrammetry. *Remote Sens. (Basel)* 7 (12), 16883–16900.
- Fodrie, F.J., Rodriguez, A.B., Baillie, C.J., Brodeur, M.C., Coleman, S.E., Gittman, R.K., Keller, D.A., Kenworthy, M.D., Poray, A.K., Ridge, J.T., Theuerkauf, E.J., Lindquist, Niels, L., 2014. Classic paradigms in a novel environment: inserting food web and productivity lessons from rocky shores and saltmarshes into biogenic reef restoration. *J. Appl. Ecol.* 51 (5), 1314–1325. <https://doi.org/10.1111/1365-2664.12276>.
- Fodrie, F.J., Rodriguez, A.B., Gittman, R.K., Grabowski, J.H., Lindquist, Niels, L., Peterson, C. H., Piehler, M. F., & Ridge, J. T., 2017. Oyster reefs as carbon sources and sinks. *Proc. R. Soc. B Biol. Sci.* 284 (1859), 20170891. <https://doi.org/10.1098/rspb.2017.0891>.
- Gallop, S.L., Vila-Concejo, A., Fellowes, T.E., Harley, M.D., Rahbani, M., Largier, J.L., 2020. Wave direction shift triggered severe erosion of beaches in estuaries and bays with limited post-storm recovery. *Earth Surf. Process. Landf.* 45 (15), 3854–3868. <https://doi.org/10.1002/esp.5005>.
- Garner, N., Ross, P.M., Falkenberg, L.J., Seymour, J.R., Siboni, N., Scanes, E., 2022. Can seagrass modify the effects of ocean acidification on oysters? *Mar. Pollut. Bull.* 177, 113438. <https://doi.org/10.1016/j.marpolbul.2022.113438>.
- Gillies, C.L., Castine, S.A., Alleway, H.K., Crawford, C., Fitzsimons, J.A., Hancock, B., Koch, P., McAfee, D., McLeod, I.M., zu Ermgassen, P. S. E., 2020. Conservation status of the Oyster Reef Ecosystem of Southern and Eastern Australia. *Global Ecology and Conservation* 22, e00988. <https://doi.org/10.1016/j.GECCO.2020.E00988>.
- Grabowski, J.H., Brumbaugh, R.D., Conrad, R.F., Keeler, A.G., Opaluch, J.J., Peterson, C. H., Piehler, M.F., Powers, S.P., Smyth, A.R., 2012. Economic Valuation of Ecosystem Services provided by Oyster Reefs. *Bioscience* 62, 900–909.
- Gutiérrez, J.L., Jones, C.G., Strayer, D.L., Iribarne, O.O., 2003. Mollusks as ecosystem engineers: the role of shell production in aquatic habitats. *Oikos* 101 (1), 79–90.
- Halpern, B.S., Walbridge, S., Selkoe, K.A., Kappel, C., v., Micheli, F., D'Agrosa, C., Bruno, J. F., Casey, K. S., Ebert, C., Fox, H. E., Fujita, R., Heinemann, D., Lenihan, H. S., Madin, E. M. P., Perry, M. T., Selig, E. R., Spalding, M., Steneck, R., & Watson, R., 2008. A Global Map of Human Impact on Marine Ecosystems. *Science* 319 (5865), 948–952. <https://doi.org/10.1126/science.1149345>.
- Harley, M.D., Turner, L.L., Short, A.D., Ranasinghe, R., 2010. Interannual variability and controls of the Sydney wave climate. *Int. J. Climatol.* 30, 1322–1335. <https://doi.org/10.1002/joc.1962>.
- Harvey, M.E., Giddings, S.N., Pawlak, G., et al., 2013. Hydrodynamic Variability of an Intermittently Closed Estuary over Interannual, Seasonal, Fortnightly, and Tidal Timescales. *Estuaries and Coasts* 46, 84–108. <https://doi.org/10.1007/s12237-021-01014-0>.
- Hearn, C.J., 2011. Hydrodynamics of Coral Reef Systems. In: Hopley, D. (Ed.), *Encyclopedia of Modern Coral Reefs. Encyclopedia of Earth Sciences Series*. Springer, Dordrecht. [https://doi.org/10.1007/978-90-481-2639-2\\_277](https://doi.org/10.1007/978-90-481-2639-2_277).
- Holthuijsen, L.H., 2007. Waves in Ocean and Coastal Waters. Cambridge University Press. <https://doi.org/10.1017/CBO9780511618536>.
- Hughes, M.G., Rogers, K., Wen, L., 2019. Saline wetland extents and tidal inundation regimes on a micro-tidal coast, New South Wales, Australia. *Estuar. Coast. Shelf Sci.* 227, 106297. <https://doi.org/10.1016/j.ecss.2019.106297>.
- Jahan, S., Strezov, V. (2019) Assessment of trace elements pollution in the sea ports of New South Wales (NSW), Australia using oysters as bioindicators. *Sci. Rep.* 9, 1416. <https://doi.org/10.1038/s41598-018-38196-w>.
- Kench, P.S., 1999. Geomorphology of Australian estuaries: review and prospect. *Aust. J. Ecol.* 24, 367–380.
- Kennedy, D.M., 2016. Estuarine Geomorphology, p. 273. [https://doi.org/10.1007/978-94-017-8801-4\\_343](https://doi.org/10.1007/978-94-017-8801-4_343).
- Kitsikoudis, V., Kibler, K.M., Walters, L.J., 2020. In-situ measurements of turbulent flow over intertidal natural and degraded oyster reefs in an estuarine lagoon. *Ecol. Eng.* 143, 105688. <https://doi.org/10.1016/j.ecoleng.2019.105688>.
- Kumbier, K., Carvalho, R.C., Vafeidis, A.T., Woodroffe, C.D., 2018. (2018) investigating compound flooding in an estuary using hydrodynamic modelling: a case study from the Shoalhaven River, Australia. *Natural Hazards Earth System. Sci.* 18, 463–477. <https://doi.org/10.5194/nhess-18-463-2018>.
- La Peyre, M.K., Serra, K., Joyner, T.A., Humphries, A., 2015. Assessing shoreline exposure and oyster habitat suitability maximizes potential success for sustainable shoreline protection using restored oyster reefs. *PeerJ* 3, e1317. <https://doi.org/10.7717/peerj.1317>.
- Lemasson, A.J., Fletcher, S., Hall-Spencer, J.M., Knights, A.M., 2017. Linking the biological impacts of ocean acidification on oysters to changes in ecosystem services: a review. *J. Exp. Mar. Biol. Ecol.* 492, 49–62.
- Leong, R.C., Bugnot, A.B., Marzinelli, E.M., Figueira, W.F., Erickson, K.R., Poore, A.G.B., Gribben, P.E., 2022. Variation in the density and body size of a threatened foundation species across multiple spatial scales. *Restoration Ecology* 30 (8), 13670.
- Marshall, D.A., Cox, N.C., la Peyre, M.K., Walton, W.C., Rikard, F.S., Pollack, J.B., Kelly, M.W., la Peyre, J.F., 2021. Tolerance of northern Gulf of Mexico eastern oysters to chronic warming at extreme salinities. *J. Therm. Biol.* 100, 103072. <https://doi.org/10.1016/j.jtherbio.2021.103072>.
- Masselink, G., Hughes, M., Knight, J., 2011. *Introduction to Coastal Processes and Geomorphology*. Taylor & Francis Group.
- Meyer, D.L., Townsend, E.C., Thayer, G.W., 1997. Stabilization and Erosion Control Value of Oyster Cultch for Intertidal Marsh. *Restor. Ecol.* 5 (1), 93–99. <https://doi.org/10.1046/j.1526-100X.1997.09710.x>.

- Morris, R.L., la Peyre, M.K., Webb, B.M., Marshall, D.A., Bilkovic, D.M., Cebrian, J., McClenachan, G., Kibler, K.M., Walters, L.J., Bushek, D., Sparks, E.L., Temple, N.A., Moody, J., Angstadt, K., Goff, J., Boswell, M., Sacks, P., Swearer, S.E., 2021. Large-scale variation in wave attenuation of oyster reef living shorelines and the influence of inundation duration. *Ecol. Appl.* 31 (6) <https://doi.org/10.1002/eap.2382>.
- North, E., Schlag, Z., Hood, R., Li, M., Zhong, L., Gross, T., Kennedy, V., 2008. Vertical swimming behavior influences the dispersal of simulated oyster larvae in a coupled particle-tracking and hydrodynamic model of Chesapeake Bay. *Mar. Ecol. Prog. Ser.* 359, 99–115. <https://doi.org/10.3354/meps07317>.
- NSW Department of Planning and Environment, 2016. *Estuaries of NSW*.
- Quan, W., Zhu, J., Ni, Y., Shi, L., Chen, Y., 2009. Faunal utilization of constructed intertidal oyster (*Crassostrea rivularis*) reef in the Yangtze River estuary, China. *Ecological Engineering* 35 (10), 1466–1475. <https://doi.org/10.1016/j.ecoleng.2009.06.001>.
- Rahbani, M., Vila-Concejo, A., Fellowes, T.E., Gallop, S.L., Winkler-Prins, L., Largier, J.L., 2022. Spatial patterns in wave signatures on beaches in estuaries and bays. *Geomorphology* 398, 108070. <https://doi.org/10.1016/j.geomorph.2021.108070>.
- Reid, D.J., 2020. A review of intensified land use effects on the ecosystems of Botany Bay and its rivers, Georges River and Cooks River, in southern Sydney, Australia. *Regional Studies in Marine Science*. 39, 101396.
- Ridge, J.T., Rodriguez, A.B., Fodrie, F.J., 2017. Salt Marsh and Fringing Oyster Reef Transgression in a Shallow Temperate Estuary: Implications for Restoration, Conservation and Blue Carbon. *Estuaries and Coasts* 40, 1013–1027. <https://doi.org/10.1007/s12237-016-0196-8>.
- Roy, P.S., 1994. Holocene estuary evolution—stratigraphic studies from Southeastern Australia. In: *Incised-Valley Systems: Origin and Sedimentary Sequences*. SEPM Society for Sedimentary Geology. <https://doi.org/10.2110/pec.94.12.0241>.
- Roy, P.S., Thom, B.G., Wright, L.D., 1980. Holocene sequences on an embayed high-energy coast: an evolutionary model. *Sediment. Geol.* 26 (1–3), 1–19. [https://doi.org/10.1016/0037-0738\(80\)90003-2](https://doi.org/10.1016/0037-0738(80)90003-2).
- Roy, P.S., Williams, R.J., Jones, A.R., Yassini, I., Gibbs, P.J., Coates, B., West, R.J., Scanes, P.R., Hudson, J.P., Nichol, S., 2001. Structure and Function of South-east Australian Estuaries. *Estuar. Coast. Shelf Sci.* 53 (3), 351–384. <https://doi.org/10.1006/ecss.2001.0796>.
- Ryan, D., Heap, A., Radke, L., Heggie, D., 2003. Conceptual models of Australia's estuaries and coastal waterways: applications for coastal resource management. *Geoscience Australia* 09, 136.
- Salvador de Paiva, J.N., Walles, B., Ysebaert, T., Bouma, T.J., 2018. Understanding the conditionality of ecosystem services: the effect of tidal flat morphology and oyster reef characteristics on sediment stabilization by oyster reefs. *Ecol. Eng.* 112, 89–95. <https://doi.org/10.1016/j.ecoleng.2017.12.020>.
- Short, A., Trenaman, N., 1992. Wave climate of the Sydney region, an energetic and highly variable ocean wave regime. *Mar. Freshw. Res.* 43 (4), 765. <https://doi.org/10.1071/MF9920765>.
- Shumway, S., Newell, R.I.E., Eble, A.F., Kennedy, V.S., 1996. *Natural environmental factors*. In: *The Eastern Oyster Crassostrea virginica*. Maryland Sea Grant College, pp. 467–513.
- Smith, K.A., North, E.W., Shi, F., et al., 2009. Modeling the Effects of Oyster Reefs and Breakwaters on Seagrass Growth. *Estuaries and Coasts* 32, 748–757. <https://doi.org/10.1007/s12237-009-9170-z>.
- Spicer, P., Huguenard, K., Ross, L., Rickard, L.N., 2019. High-Frequency Tide-Surge-River Interaction in Estuaries: Causes and Implications for Coastal Flooding. *J. Geophys. Res. Oceans* 124 (12), 9517–9530. <https://doi.org/10.1029/2019JC015466>.
- Spooner, D., Maher, W., Otway, N., 2003. Trace Metal Concentrations in Sediments and Oysters of Botany Bay, NSW, Australia. *Arch. Environ. Contam. Toxicol.* 45, 0092–0101. <https://doi.org/10.1007/s00244-002-0111-0>.
- Stagličić, N., Šegvić-Bubić, T., Ezgeta-Balić, D., Bojanić Varezić, D., Grubišić, L., Žuvić, L., Lin, Y., Briski, E., 2020. Distribution patterns of two co-existing oyster species in the northern Adriatic Sea: the native European flat oyster *Ostrea edulis* and the non-native Pacific oyster *Magallana gigas*. *Ecol. Indic.* 113, 106233 <https://doi.org/10.1016/j.ecolind.2020.106233>.
- Taylor, M.D., Baker, J., Suthers, M.I., 2013. Tidal currents, sampling effort and baited remote underwater video (BRUV) surveys: are we drawing the right conclusions? *Fish. Res.* 140, 96–104. <https://doi.org/10.1016/j.fishres.2012.12.013>.
- Theuerkauf, S.J., Eggleston, D.B., Puckett, B.J., Theuerkauf, K.W., 2017. Wave Exposure Structures Oyster distribution on Natural Intertidal Reefs, but not on Hardened Shorelines. *Estuaries and Coasts* 40 (2), 376–386. <https://doi.org/10.1007/s12237-016-0153-6>.
- Tolley, G., Volety, A., 2005. The role of oysters in habitat use of oyster reefs by resident fishes and decapod crustaceans. *J. Shellfish. Res.* 24 (4), 1007–1012.
- Vila-Concejo, A., Gallop, S.L., Largier, J.L., 2020. Sandy beaches in estuaries and bays. In: *Sandy Beach Morphodynamics*. Elsevier, pp. 343–362. <https://doi.org/10.1016/B978-0-08-102927-5.00015-1>.
- Wall, L., Walters, L., Grizzle, R., Sacks, P., 2005. *Recreational Boating Activity and its Impact on the Recruitment and Survival of the Oyster Crassostrea virginica on Intertidal Reefs in Mosquito Lagoon, Florida*. Faculty Bibliography.
- Walles, B., Salvador de Paiva, J., van Prooijen, B.C., Ysebaert, T., Smaal, A.C., 2014. The Ecosystem Engineer *Crassostrea gigas* Affects Tidal Flat Morphology beyond the Boundary of their Reef Structures. *Estuaries and Coasts* 38, 941–950. <https://doi.org/10.1007/s12237-014-9860-z>.
- Whitman, E.R., Matthew, A.R., 2012. Benthic flow environments affect recruitment of *Crassostrea virginica* larvae to an intertidal oyster reef. *Mar. Ecol. Prog. Ser.* 463, 177–191.
- Wiberg, P.L., Taube, S.R., Ferguson, A.E., Kremer, M.R., Reidenbach, M.A., 2019. Wave Attenuation by Oyster Reefs in Shallow Coastal Bays. *Estuar. Coasts* 42 (2), 331–347. <https://doi.org/10.1007/s12237-018-0463-y>.
- Wright, A.E., 1976. *Review of the Origin and Evolution of the Benue Trough in Nigeria (Department of Earth Sciences)*.
- Zhu, L., Chen, Q., Wang, H., Capurso, W., Niemoczynski, L., Hu, K., Snedden, G., 2020. Field Observations of Wind Waves in Upper Delaware Bay with living Shorelines. *Estuaries and Coasts* 43 (4), 739–755. <https://doi.org/10.1007/s12237-019-00670-7>.
- zu Ermgassen, P.S.E., Spalding, M.D., Grizzle, R.E., et al., 2013. Quantifying the loss of a Marine Ecosystem Service: Filtration by the Eastern Oyster in US Estuaries. *Estuaries and Coasts* 36, 36–43. <https://doi.org/10.1007/s12237-012-9559-y>.